Journal of Ceramic Processing Research. Vol. 25, No. 4, pp. 643~659 (2024)
(Received 14 April 2024, Received in revised form 17 June 2024, Accepted 5 July 2024)
https://doi.org/10.36410/jcpr.2024.25.4.643

J O U R N A L O F
Ceramic Processing Research

Study on motorized spindle with full ceramic ball bearings and lubrication at high speeds

Yonghua Wang[a], Songhua Li[a,b,*], Chao Wei[c], Yu Zhang[a], Gefei Lin[a], Dong An[a] and Jining Zhao[a]
[a]*School of Mechanical Engineering, Shenyang Jianzhu University, Shenyang 110168, China*
[a]*National-Local Joint Engineering Laboratory of NC Machining Equipment and Technology of High-Grade Stone, Shenyang 110168, China*
[c]*School of Engineering Training and Innovation, Shenyang Jianzhu University, Shenyang 110168, China*

The lubrication methods and material characteristics of high-speed rolling bearings significantly impact the vibration and temperature of motorized spindles in high-speed machine tools. This study focuses on replacing traditional metal bearings with full ceramic ball bearings and analyzes three different types of bearings: Si_3N_4-Si_3N_4, ZrO_2-Si_3N_4, and GCr15-GCr15. Based on the quasi-static and oil film thickness theory of bearing, the influence of rotational speed on the centrifugal force of bearings of different materials and the oil film thickness of the raceway center of inner and outer rings was analyzed. According to different lubrication methods, the vibration and temperature rise characteristics of motorized spindle bearing systems under high-speed working conditions are analyzed in experiment. The results indicate that Si_3N_4-Si_3N_4 bearings exhibit lower centrifugal force and thicker oil films than the others. The experimental results show that the vibration-effective value of the Si_3N_4-Si_3N_4 bearing is lower than that of the other two materials when the speed is higher. Grease lubrication slightly reduces vibration acceleration compared to oil-air lubrication. The temperature rise difference of motorized spindle of oil-air lubricated full ceramic bearings is smaller than that of grease lubrication, and the average temperature rise difference is 4°C. Full ceramic bearings outperform steel bearings in all aspects under the same working conditions, and the Si_3N_4-Si_3N_4 bearing embodies the advantages of dynamic and thermal performance.

Keywords: Full ceramic ball bearings, High-speed motorized spindle, Lubrication methods, Vibration characteristics, Temperature rise characteristic.

Introduction

With the rapid development of the advanced machinery manufacturing industry, the products processed by high-speed motorized spindles have been widely used in the fields of machinery, electronics, chemical industry, military, aerospace and bioengineering and other high-precision processing fields due to their high processing accuracy and efficiency [1-3]. As the core structural unit of advanced CNC machine tools, the motorized spindle's operation accuracy determines the machined parts' accuracy, and the machining accuracy represents the development direction of future advanced manufacturing technology [4]. As a key core supporting component of the spindle of CNC machine tools, rolling bearings, whose D_mN value of the product of the bearing pitch diameter and speed is mostly more than 1×10^6 mm·(r/min), can be called high-speed bearings [5]. Bearing failure under high-speed conditions is the main form of vibration and temperature rise [6], which, as an important index to evaluate the performance of the motorized spindle system, directly affects the stability and fatigue life of the motorized spindle [7, 8]. Therefore, it is particularly important to monitor the vibration and temperature rise of motorized spindle bearings.

When the traditional steel ball bearing runs at high speed, it produces enormous centrifugal force and gyro torque, sharply increasing the contact stress between the rolling body and the bearing's outer ring. The steel material is affected by thermal expansion and cold contraction, and the bearing hardness is difficult to maintain, resulting in increased bearing deformation. Due to the extrusion of the internal lubricant, the oil film thickness decreases, the oil film carrying capacity decreases, and it is more likely to lead to the failure of lubricating oil. The increase in friction coefficient generates a large amount of friction heat, aggravates bearing vibration and temperature rise, and the bearing is prone to fatigue failure, which will exacerbate the failure of the bearing. Therefore, steel ball bearings are no longer the best choice to be applied to the motorized spindle under high-speed working conditions [9, 10]. Due to the advantages of low density, small thermal expansion coefficient, significant elastic modulus, and

*Corresponding author:
Tel : +86-136 0407 0287
Fax: 024-24692196
E-mail: lisonghua@sjzu.edu.cn

self-lubrication, engineering ceramic materials have excellent performance when applied to rolling bearings at high speed and high-temperature conditions, reducing the centrifugal force and gyroscope moment of the ball, significantly improving the speed, stiffness, and life of the motorized spindle [11]. Therefore, studying the vibration and temperature rise of full ceramic ball bearings under different speed and lubrication methods is of great significance.

Many scholars have recently conducted research on motorized spindle bearing systems' vibration and temperature rise from different angles according to the actual working conditions. Cao et al. [12-14] concluded that bearing vibration is related to the interaction between various components and is affected by working condition parameters. Jamadar et al. [15] studied the influence of grease viscosity on mechanical vibration related to bearings when they are damaged, and the results showed that when the grease viscosity was high, the bearing amplitude was lower, thus improving the service performance of bearings. Wang et al. [16, 17] established a thermo-mechanical fully coupled bearing model, calculated and analyzed the temperature and axial deformation of bearings at different rotational speeds, and then obtained the change law of dynamic and thermal characteristics of bearings. Hao Xu et al. [18] built a test bed for a single-disc rotor-bearing system with two fulcrum, measured and analyzed the displacement and acceleration of the support end of cylindrical roller bearings with eddy current and acceleration sensors, and studied the vibration response of the rotor during the process of bearing heat balance and under different lubricating oil temperatures. Wu Yuhou et al. [19] conducted lubrication vibration characteristics experiments on full ceramic bearings by changing preload forces and oil supply. They established a dynamic model of full ceramic deep groove ball bearings under lubrication conditions. Zhang Ke et al. [20] established a dynamic thermal coupling model of a ceramic motorized spindle bearing system to determine the optimal preload at different speeds and studied the effects of speed, preload, and thermal deformation on bearing vibration characteristics. Bai Xiaotian et al. [21, 22] established an full ceramic bearing model considering ball diameter difference. They later studied the vibration characteristics of full ceramic bearings under oil absence.

Zheng et al. [23] established a thermal expansion load balance model of angular contact ball bearings to calculate bearing load changes and study the relationship between heat generation and heat transfer in the rotating shaft, considering the constraints of coolant, radial, and axial structure. Wu Li et al. [24] established the heat transfer model of angular contact ball bearing by finite element method based on the bearing pseudo-static method and bearing heat generation theory, explored the influence of temperature rise on the heat displacement of bearing components, and analyzed the variation law between different speed, load and bearing temperature field. Wu et al. [25] established angular contact ball bearings' differential sliding heat generation based on Elastohydrodynamic Lubrication (EHL) theory. The study takes into account the asperity elastic-plastic deformation, establishing an improved model with high accuracy in verifications with experimental data and existing model. Other aspects, such as bearing structure size, surface waviness, number of rolling elements, backlash, and cage [26-30], have also been extensively studied on the influence of bearing load, oil-air lubrication flow field, rotation accuracy, friction and other fields on the bearing thermal characteristics [31], and practical conclusions have been drawn.

To sum up, the current research on the factors affecting vibration and temperature rise of motorized spindle bearing systems has achieved extensive and in-depth research results and has achieved many valuable results. There are some research results have been obtained at high speed on the vibration and temperature rise characteristics of motorized spindle systems equipped with metal bearings. However, the research on the effects of vibration and temperature rise on motorized spindle systems equipped with different materials is still in its infancy in related fields, and experimental research is lacking. Starting with the full ceramic bearing motorized spindle, this paper uses the bearing quasi-static theory and the oil film thickness theory to obtain accurate numerical solutions through Newton's method to analyze the influence of rotational speed on the centrifugal force and the oil film thickness of the center of the raceway of the inner and outer rings of the bearing. In addition, the dynamic and thermal performance tests of the full ceramic bearing motorized spindle of different materials are carried out at different speeds and under different lubrication methods under high-speed working conditions. The test results verify the service performance advantages of the full ceramic bearing under high-speed conditions, improve the comprehensive performance of the motorized spindle, and the results of the vibration and temperature rise of the full ceramic bearing have guiding significance for the design theory of the full ceramic bearing motorized spindle. They can effectively promote the development of the national equipment manufacturing industry.

Experimental Research

Experimental motorized spindle bearing selection and assembly

The motorized spindle-bearing system adopted in this experiment is based on the high-speed motorized spindle model SJZU170-30/15, and the performance parameters are shown in Table 1. Before conducting the experiment, the motorized spindle needs to be mounted with bearings made of three different materials, respectively. The bearings used in the test are full ceramic angular contact ball bearings (model: 7009C, rolling body material is

Table 1. Performance parameters of the spindle

Parameters	Values
Rated speed (r/min)	30000
Rated voltage(V)	350
Rated frequency(Hz)	500
Rated current (A)	19
Rated power (kW)	15
Pole logarithm	4

Si_3N_4, inner and outer ring material is Si_3N_4, ZrO_2) and steel angular contact ball bearing (model: 7009C, the rolling body and the inner and outer rings are GCr15), the cage is made of PEEK composite material for comparison, the bearings are located at both ends of the motorized spindle, the motorized spindle is placed on the test bench, the inner ring rotates with the rotating shaft, the outer ring is fixed with the bearing seat, the bearing accuracy is P4, the ball accuracy reaches G3.

As can be seen, due to the relatively complex structure of the motorized spindle, in order not to affect the operation accuracy of the motorized spindle after bearing assembly, each component of the motorized spindle needs to be cleaned with gasoline and dried naturally before assembling. The assembly sequence is as follows: first, the large front cover of the motorized spindle is used, and then the front and rear bearings are installed. The bearings are installed in pairs with their faces facing each other, and lubricating oil is evenly applied to each bearing prior to installation. The interference between the steel bearing and the rotating shaft is small, it can be assembled by direct pressing, which will affect the rotation accuracy of the bearing, so the ceramic bearing needs to be installed in liquid nitrogen cold state.The interference amount is approximately 1-2 micrometers, and then the linear bearing and the bearing seat are installed, and the six springs are installed at the same time. The rear end lock cap and the rear cover are installed. The assembled high-speed motorized spindle and bearing test bench are shown in Fig. 1.

In this paper, angular contact ball bearing 7009C is been used as an example, also the performance of bearing in different materials is analyzed. The bearing structural parameters and material characteristics are shown in Table 2 and Table 3.

Experimental scheme and process

As shown in Fig. 2, the high-speed motorized spindle bearing test bench is composed of four parts: control system, detection system, water cooling system and

Table 2. Structure parameters of 7009C bearing

Bearing type	7009C
Bearing bore diameter d/mm	45
Contact Angle	15°
Number of balls Z/n	17
Bearing outside diameter D/mm	75
Bearing width B/mm	16
Ball diameter D_b/mm	8.731
Pitch diameter D_m/mm	60
Curvature radius of inner ring raceway f_i/mm	0.515
Curvature radius of outer ring raceway f_e/mm	0.525

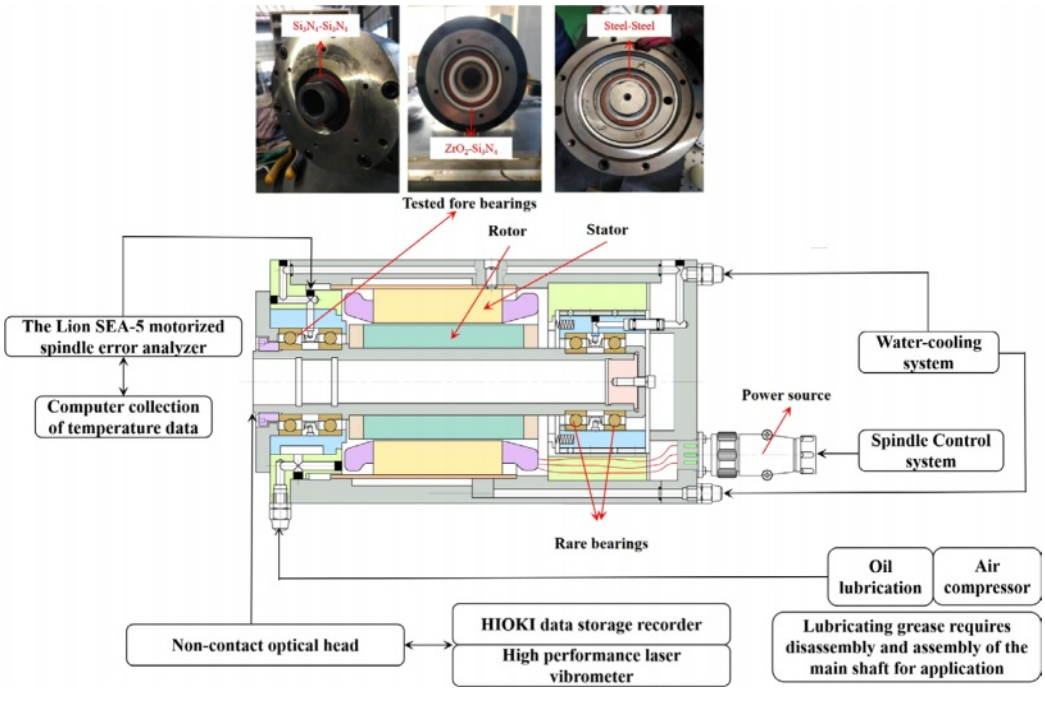

Fig. 1. Schematic of the test bench composition.

Table 3. Material parameters of the 7009C bearing

Bearing Material	Si_3N_4	ZrO_2	GCr15
Elastic Modulus(GPa)	310	195	207
Poisson's Ratio	0.26	0.3	0.3
Density(g/cm^3)	3.24	5.88	7.85
Coefficient of thermal expansion (k^{-1})	3.2	8.75	3
Termal conductivity (w $m^{-1}k^{-1}$)	35	3	45

lubrication system. The test bench is operated by the motorized spindle bearing performance test system. The spindle speed is controlled by conputer, also the loading load can be setted.. By changing those two parameters, a series of tests are conducted on the motorized spindle. The detection system utilizes the OFV-5000 Xtra high performance laser Vibration meter of German POLYTEC and the MLV-I-120 Xtra optical head. This device uses non-contact sensor to collect vibration signals at the spindle end, which can realize the simultaneous output of vibration displacement, speed and acceleration signals in multiple channels. Time domain and frequency domain analysis, measuring distance range 0.5~100 m, maximum speed ±25 m/s, available frequency range 0.5~5 kHz. The temperature sensors are placed on the front and rear bearing housing of the high-speed motorized spindle, the temperature distribution of the outer ring of the bearing is detected by Lion SEA-5 motorized spindle error analyzer.

The experiment was conducted in a dust-free laboratory with an ambient temperature of 25°C±2°C and humidity no greater than 75%. The test was conducted under no-load conditions. The lubrication conditions included oil and gas lubrication as well as grease lubrication. The model of the oil and gas lubrication system was MIXAIR2, and the compressed air pressure for the lubrication system was maintained at a constant 0.36 MPa during the experiment. The water cooling system maintained a constant water temperature of 18°C, with a flow rate of 170 ml/s.

The vibration and temperature rise of the bearing were studied using the control variable method. The speed of the motorized spindle was altered while maintaining constant lubrication methods, unchanged bearing material, and a preload of 400N. High-speed bearings generally refer to bearings with a speed value greater than 1×10^6 r/min. In the case of 7009C bearings with d_m=60, the required speed must exceed 16666 r/min. Since the speed starts from a high level, before reaching the test speed, the spindle speed is gradually increased to the tested speed, with each increment of 1000 r/min. The test starts at 18000 r/min and continues up to 30000 r/min. After each group reaches the target speed, the motorized spindle maintains the speed for 1 hour. Due to the large number of experimental groups, 7 groups of effective vibration values and 5 groups of vibration frequency domain and temperature rise speed conditions were selected for further analysis. The experimental flow chart is shown in Fig. 3, and the experimental scheme is shown in Table 4.

Theoretical Model of Full Ceramic Ball Bearing

Geometry of internal deformation of full ceramic ball bearing elements

Figure 4 shows the structure diagram of the full ceramic ball bearing. The full ceramic ball bearing consists of an inner and outer ring, a cage, and rolling elements. During the working process of the bearing,

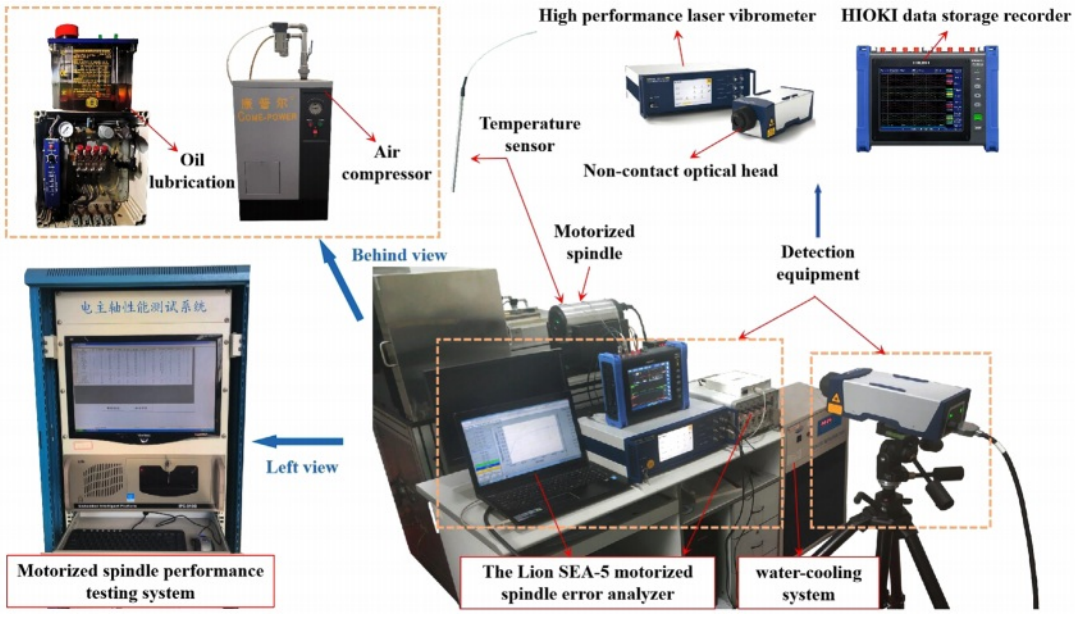

Fig. 2. High speed motorized spindle-bearing test bench.

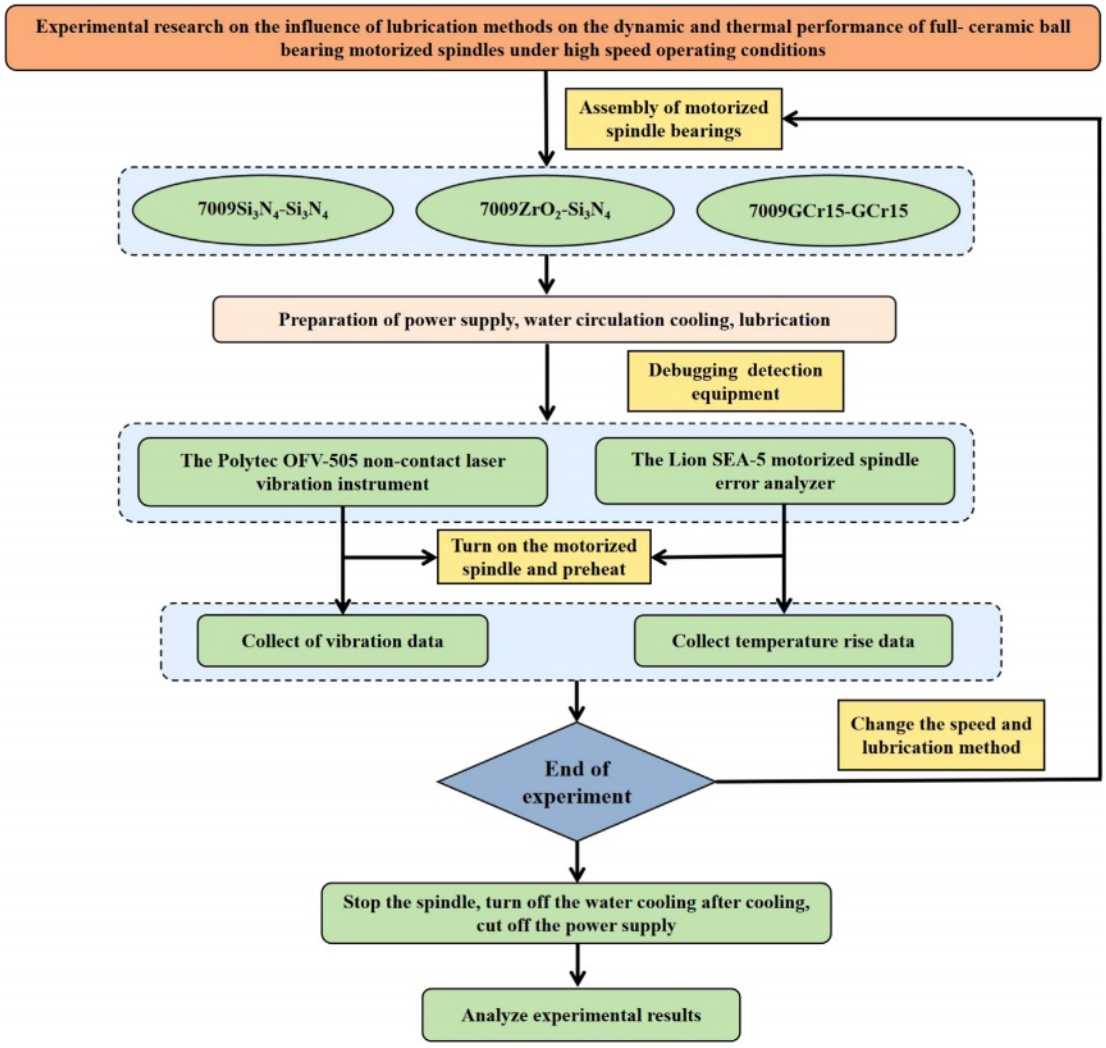

Fig. 3. Experimental flow chart.

Table 4. Experimental scheme for the effect of lubrication methods on the performance of bearings made of different materials under high-speed working conditions

Test group	Bearing material	Rotational speed(r/min)	Preload(N)	Lubrication method	Test time(min)
1	Si_3N_4-Si_3N_4	18000-30000 (The value increases by 1000r/min)	400	Oil-air lubrication	60min
2	ZrO_2-Si_3N_4			Grease lubrication	
3	GCr15-GCr15				

the inner ring is installed on the rotating shaft, and the outer ring is installed in the bearing seat. Usually, the inner ring and the rotating shaft have an interference fit; the outer ring and the bearing seat have a gap fit, so the inner ring rotates, and the outer ring remains stationary. Meanwhile, B represents the bearing width, d and D are the diameters of the inner and outer rings of the bearing, respectively, d_i and D_e are the bottom diameters of the inner and outer rings of the bearing, respectively, d_m is the diameter of the bearing pitch diameter, D_b is the diameter of the ceramic ball, α_0 is the initial contact angle, C_r is the radial clearance of the bearing.

As shown in Fig. 4, r_i and r_e are the radius of curvature of the inner and outer rings, respectively.

$$\begin{cases} r_i = f_i D_b \\ r_e = f_e D_b \end{cases} \tag{1}$$

$$\gamma = \frac{D_b \cos\alpha}{d_m} \tag{2}$$

Where, γ is a dimensionless geometric parameter; f_i and f_e are the coefficient of raceway curvature radius of the inner and outer rings respectively.

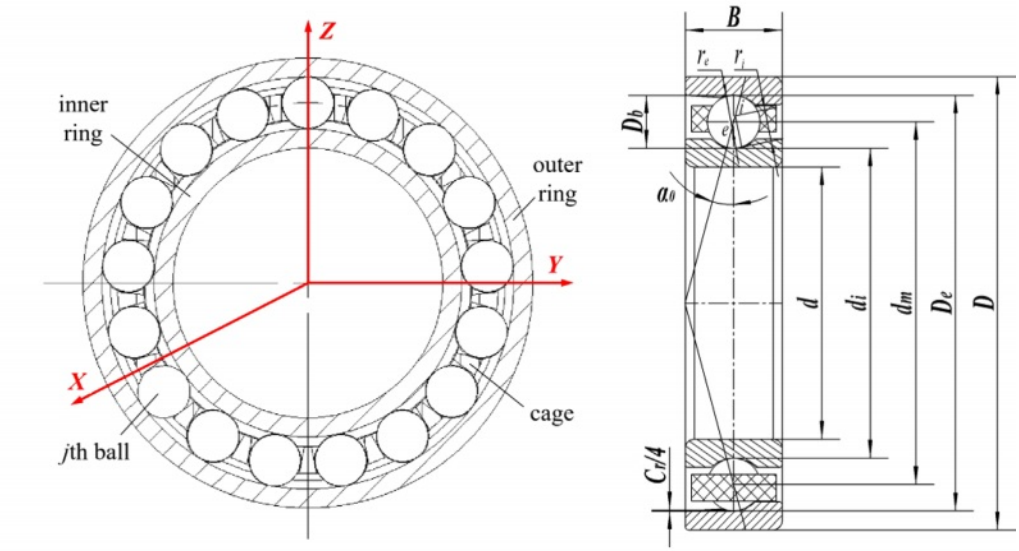

Fig. 4. 7009C Structure diagram of full ceramic ball bearing.

The pitch diameter of the bearing is equal to the average of the diameter of the inner and outer rings:

$$d_m = 0.5(d + D) \tag{3}$$

The initial bearing contact Angle α, is determined by the structural design parameters and the original clearance:

$$\alpha = \arccos(1 - \frac{C_r}{2A}) \tag{4}$$

Where, A is the distance between the center of curvature of the inner and outer ring raceway, which is determined by the following formula:

Inner and outer raceway center of curvature locus circle radius:

$$r_i = 0.5d_m + D_b(f_i - 0.5)\cos\alpha \tag{5}$$

$$r_e = 0.5d_m - D_b(f_e - 0.5)\cos\alpha \tag{6}$$

Calculating formula of diameter of inner and outer raceway of ball bearing [32]:

$$d_i = d_m - D_b\left[2f_e - (2f_e - 1)\cos\alpha\right] \tag{7}$$

$$D_e = d_m + D_b\left[2f_e - (2f_e - 1)\cos\alpha\right] \tag{8}$$

When the full ceramic ball bearing is applied in high-speed conditions, the centrifugal force and gyroscopic torque generated by the high speed cause elastic deformation of the bearing under the combined action of the two forces. This deformation further results in changes to the bearing rolling center and the curvature centers of the inner and outer ring raceways, altering their relative positions so that they are no longer collinear.

In this paper, full ceramic ball bearings are applied to high-speed motorized spindles. The inner ring rotates with the rotating shaft, while the outer ring is fixed with the bearing seat. Therefore, the O_e of the groove curvature center of the outer raceway is fixed, and the load movement relationship between the O_i of the groove curvature center of the inner raceway and the O_b of the ball is shown in Fig. 5 [33]. For the J-th rolling element, X_{1j} and X_{2j} are the relative positions of the ball center of the rolling element, representing the axial and radial distances between the ball center and the center of curvature of the outer raceway groove, respectively; A_{1j} and A_{2j} represent the axial and radial distances between the center of curvature of the inner raceway groove and the center of curvature of the outer raceway groove. According to the geometric relationship shown in Fig. 5, the expressions of A_{1j} and A_{2j} are respectively:

$$\begin{cases} A_{1j} = (f_e + f_i - 1)D_b\sin\alpha_0 + \delta_x + r_i(\theta_x\sin\varphi_j - \theta_y\cos\varphi_j) \\ A_{2j} = (f_e + f_i - 1)D_b\cos\alpha_0 + \delta_x\cos\varphi_j + \delta_y\sin\varphi_j \end{cases} \tag{9}$$

Where δ_x, δ_y and δ_z are the translational displacement of the inner ring along the X, Y and Z axes, respectively. θ_x and θ_y are angular displacements along the X and Y axes. φ_j is the azimuth Angle of the jth ball, which is calculated as follows:

$$\varphi_j = 2\pi(j-1)/Z_b \tag{10}$$

Among them, Z_b is the number of bearing rolling elements.

When the bearing rotates at high speed, elastic deformation occurs within the bearing due to the action of centrifugal force and external load. The movement of the rolling element will cause the initial contact angle α_0 to change. The contact angle between the rolling element and both the inner and outer raceways will change to α_{ij} and α_{ej} respectively. Under this working condition, the

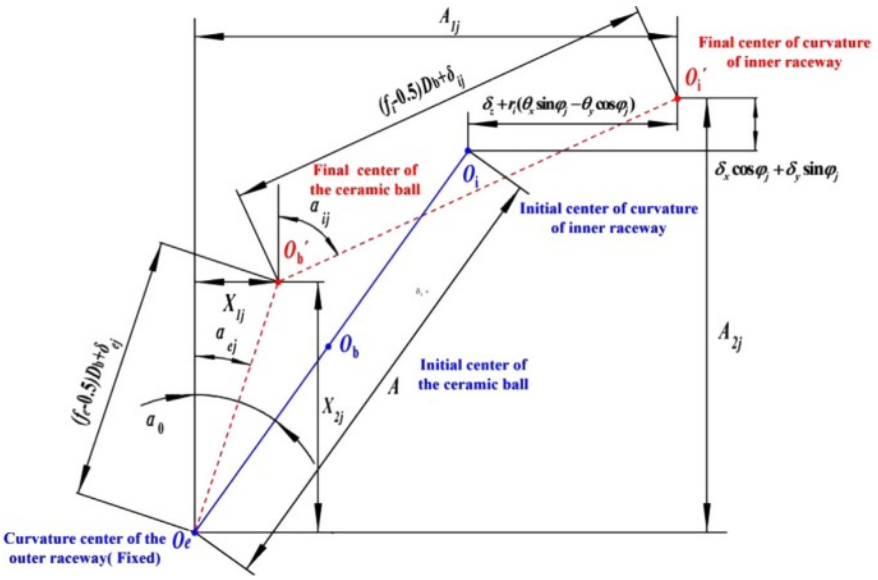

Fig. 5. Bearing internal components relative position change.

contact angle between the jth ceramic ball and the inner raceway and the outer raceway can be obtained from the position relationship in Fig. 5 [33]:

$$\alpha_{ij} = \arctan\frac{A_{1j} - X_{1j}}{A_{2j} - X_{2j}} \tag{11}$$

$$\alpha_{ej} = \arctan\frac{X_{1j}}{X_{2j}} \tag{12}$$

The geometric relation of ball center position change of ceramic bearing is shown in equation (13) and equation (14).

$$(A_{1j} - X_{1j})^2 + (A_{2j} - X_{2j})^2 - [(f_i - 0.5)D_b + \delta_{ij}]^2 = 0 \tag{13}$$

$$X_{1j}{}^2 + X_{2j}{}^2 - [(f_e - 0.5)D_b + \delta_{ej}]^2 = 0 \tag{14}$$

Force analysis of ceramic ball

The force and moment of the jth ceramic ball are shown in Fig. 6. Assuming the tangential friction force of the ceramic ball and the gyroscope moment are balanced, the force balance equation of the rolling body along the X and Z axes is [34]:

$$\begin{cases} Q_{ij}\sin\alpha_{ij} - Q_{ej}\sin\alpha_{ej} + F_{ij}\cos\alpha_{ij} - F_{ej}\cos\alpha_{ej} = 0 \\ Q_{ij}\cos\alpha_{ij} - Q_{ej}\cos\alpha_{ej} - F_{ij}\sin\alpha_{ij} + F_{ej}\sin\alpha_{ej} + F_{cj} = 0 \\ F_{ej} + F_{ij} - 2M_{gi}/D = 0 \end{cases} \tag{15}$$

The relationship between tangential friction force and normal contact load of ceramic balls can be approximately expressed as follows:

$$F_{ij/ej} = \mu_j Q_{ij/ej} \tag{16}$$

Where μ_j is the friction coefficient between the raceway and the ceramic ball.

According to the Hertz contact theory, the contact load between the ceramic ball and the inner and outer raceways can be determined through the contact elastic deformation. The process is as follows:

$$Q_{ij/ej} = K_{ij/ej}\delta_{ij/ej}^{1.5} \tag{17}$$

Where K_{ij} and K_{ej} represent the load-deformation coefficients for the ceramic ball and the inner and outer raceways, respectively.

As shown in Fig. 6, the ceramic ball rotates around the bearing axis during the working process while also rotating around its own axis, and its rotation axis is not parallel to the bearing's rotation axis. When the bearing rotates at high speed, the influence of centrifugal force F_{cj} (related to the rotating motion of the ceramic ball) and

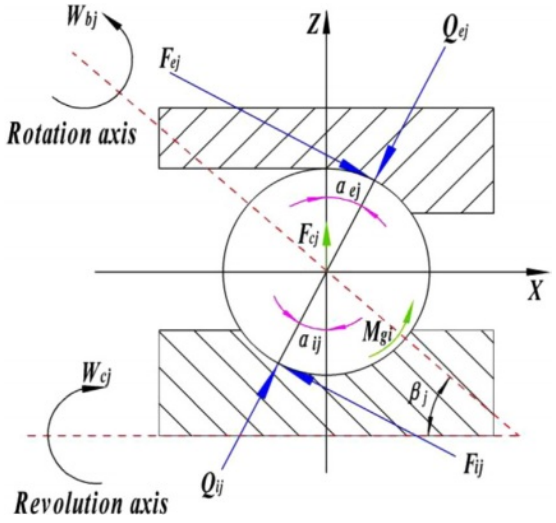

Fig. 6. Force analysis diagram of contact between ceramic ball and raceway.

gyroscopic torque M_{gj} (also related to the rotating motion of the ceramic ball) cannot be ignored. The calculation formula for these forces and torques is as follows:

$$F_{cj} = 0.5 d_m m_b w_{cj}^2 \tag{18}$$

$$M_{gi} = J_b w_{bj} w_{cj} \sin \beta_j \tag{19}$$

The mass m_b and the moment of inertia J of the ceramic ball can be obtained from equation (20)

$$\begin{cases} m = \rho \pi D_b^{\ 3} / 6 \\ J = \rho \pi D_b^{\ 5} / 60 \end{cases} \tag{20}$$

Calculation of oil film thickness under elastohydrodynamic lubrication

For full ceramic ball bearings with oval point contact, the oil film thickness between ceramic ball and inner and outer raceway is calculated using the Hamrock-Dowson [35] central oil film thickness formula.

$$\begin{cases} h_i = 2.69 R_i U_i^{0.67} M^{0.53} L_i^{-0.067} (1 - 0.61 e^{-0.73k}) \\ h_e = 2.69 R_e U_e^{0.67} M^{0.53} L_e^{-0.067} (1 - 0.61 e^{-0.73k}) \end{cases} \tag{21}$$

$R_{i/e}$ is respectively the equivalent curvature radius of the ball in contact with the inner and outer rings along the direction of the ceramic ball, which can be expressed as:

$$R_{i(e)} = \frac{r_{i/e} r_b}{r_{i/e} \pm r_b} = \frac{1}{2} D_b (1 \mp \gamma) \tag{22}$$

$U_{i/e}$ is the dimensionless velocity parameter, M is the dimensionless material parameter, $L_{i/e}$ is the dimensionless load parameter, which can be expressed as:

$$U_{i/e} = \frac{\eta_0 u}{E_0 R_{i/e}} \tag{23}$$

$$M = \alpha^* E_0 \tag{24}$$

$$L_{i/e} = \frac{Q_{ij/ej}}{E_0 R_{i/e}^2} \tag{25}$$

Where η_0 is the dynamic viscosity of the lubricating oil under normal pressure, u is the average velocity of the two contact surfaces, and is the viscous pressure coefficient, which can be calculated:

$$u = \frac{\pi n}{120} d_m (1 - \gamma^2) \tag{26}$$

$$\alpha^* = \frac{\ln \eta_0 + 9.67}{p} \left[(1 + 5.1 \times 10^{-9} p)^{0.68} \left(\frac{T - 138}{T_0 - 138} \right)^{-1.1} - 1 \right] \tag{27}$$

n is the speed of the inner ring, r/min; T_0 is the ambient temperature; T is the actual temperature of the oil film. E_0 is the comprehensive elastic modulus, and the relationship between E_0 and the elastic modulus of each rolling element is satisfied:

$$\frac{1}{E_0} = \frac{1}{2} \left(\frac{1 - \sigma_i^2}{E_i} + \frac{1 - \sigma_b^2}{E_b} \right) \tag{28}$$

Where E_i and E_b are elastic modulus of ceramic inner ring and ceramic ball respectively; And Poisson's ratio of ceramic inner ring and ceramic ball respectively; k is the ellipticity of the contact region, k=a/b.

Results and Discussion

Analysis of influence of rotational speed on centrifugal force of bearing

The influence of rotational speed on the centrifugal force of bearings made from different materials is shown in Fig. 7. With the increase in rotational speed, the centrifugal force of bearings made from all three materials increases. According to the centrifugal force calculation formula in Section 3.2, the centrifugal force of bearings of the same type is related to bearing mass and rotational speed. The density of Si_3N_4-Si_3N_4 and ZrO_2-Si_3N_4 bearings is significantly lower than that of GCr15-GCr15, resulting in much smaller bearing masses. Consequently, with increasing speed, the centrifugal force of Si_3N_4-Si_3N_4 and ZrO_2-Si_3N_4 ceramic bearings is much lower than that of GCr15-GCr15 bearings. As shown in Fig. 7, the centrifugal force of Si_3N_4-Si_3N_4 bearings exhibits a slow growth trend and remains minimal at different speeds. The centrifugal force of the ZrO_2-Si_3N_4 bearing is higher than that of the Si_3N_4-Si_3N_4 bearing, and the growth trend becomes increasingly pronounced with increasing speed. In contrast, the centrifugal force of GCr15-GCr15 bearings is significantly higher and exhibits a linear growth trend. Due to the superior hardness and wear resistance of ceramic materials compared to steel, ceramic bearings undergo minimal wear during high-speed rotation, further minimizing the wear-induced

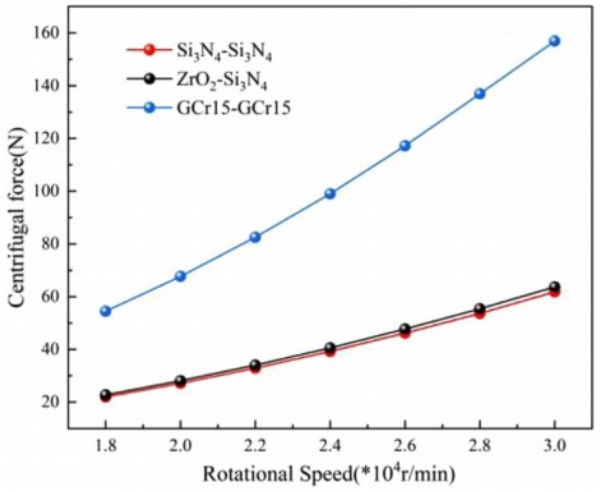

Fig. 7. Effect of rotational speed on centrifugal force of bearings of different materials.

mass increase. This maintains a low centrifugal force, enabling Si_3N_4-Si_3N_4 bearings to exhibit their performance advantages under various lubrication conditions.

Analysis of influence of working condition on vibration

The effective value X_{rms} reflects the energy of the signal, which is more suitable for the rolling bearing detection with random vibration. The greater the degree of wear of the bearing, the higher the X_{rms} value. The speed of the motorized spindle ranged from 18000 r/min to 30000 r/min. By measuring the vibration acceleration of the front bearing at various speed conditions, we processed the data using Fourier transform and calculated the effective value. The effective value refers to the energy intensity and stability of the vibration energy in a period. It can be expressed as:

$$X_{rms} = \sqrt{\frac{1}{N}\sum_{i=1}^{N} x_i^2} \tag{29}$$

The experiment was repeated three times, and the vibration effective value was obtained, as shown in Fig. 8. When the preload force is maintained at 400N, the bearing vibration effective values under different lubrication methods exhibit an increasing trend with the rise in spindle speed, as depicted in Fig. 8. The vibration RMS of the Si_3N_4-Si_3N_4 bearing increases gradually with increasing spindle speed, and the increase is most gradual within the range of 20000-22000 r/min. Compared to the Si_3N_4-Si_3N_4 bearing, the ZrO_2-Si_3N_4 and GCr15-GCr15 bearings show a more significant increase in vibration at high speeds. From the analysis of the influence of 4.1 section speed on the bearing centrifugal force, it can be seen that the centrifugal force has a great influence on the bearing vibration under high speed working condition.

As can be seen from Fig. 8(a) and (b), vibration effective values under grease lubrication are lower than those under oil-air lubrication on the whole. This may be the case for full ceramic ball bearings with oil-air lubrication. During high-speed rotation, the strong airflow from the raceway generated by centrifugal force forms a convection with the oil-air entering the bearing raceway, which prevents the lubricating oil-air from entering the bearing raceway to a certain extent and affects the lubrication of the bearing. With the increase of the spindle speed, this influence becomes more and more significant. It will lead to insufficient lubrication of the bearing raceway, thus increasing the bearing vibration. For ball bearings with grease lubrication, due to the relatively large viscosity and poor fluidity of grease, the lubricant loss in the raceway is relatively small during bearing operation, and the rolling body is sufficiently lubricated and runs smoothly. Therefore, the vibration effective acceleration value of grease lubricated bearings is slightly lower than that of oil-air lubricated bearings under high-speed working conditions.

Overall, under different lubrication methods, the vibration effective values of Si_3N_4-Si_3N_4 bearings remains relatively low at higher speeds. Under oil-air lubrication method, the vibration effective values of bearings with different materials exhibits the most significant variance at 30000 r/min, which is lower than that of ZrO_2-Si_3N_4 bearings by 23.2% and GCr15-GCr15 bearings by 33.9%. Under grease lubrication methods, it is 17.9% lower than ZrO_2-Si_3N_4 bearings and 42.6% GCr15-GCr15 bearings. The analysis shows that the bearing rolling body, cage and lubricant filled in the bearing raceway under high-speed operation have a large centrifugal force, and with the increase of the rotational speed, the centrifugal force continues to increase, a large number of lubricants will be emitted from the bearing raceway inside and out, thus affecting the lubrication state of the bearing to a certain extent. The full ceramic bearing shows excellent performance in the case of the lack of lubricant in high-speed working conditions, which shows that the ceramic material has a certain self-lubricating performance to a certain extent, and may be in low-speed working conditions, mainly the preload force plays a role, when

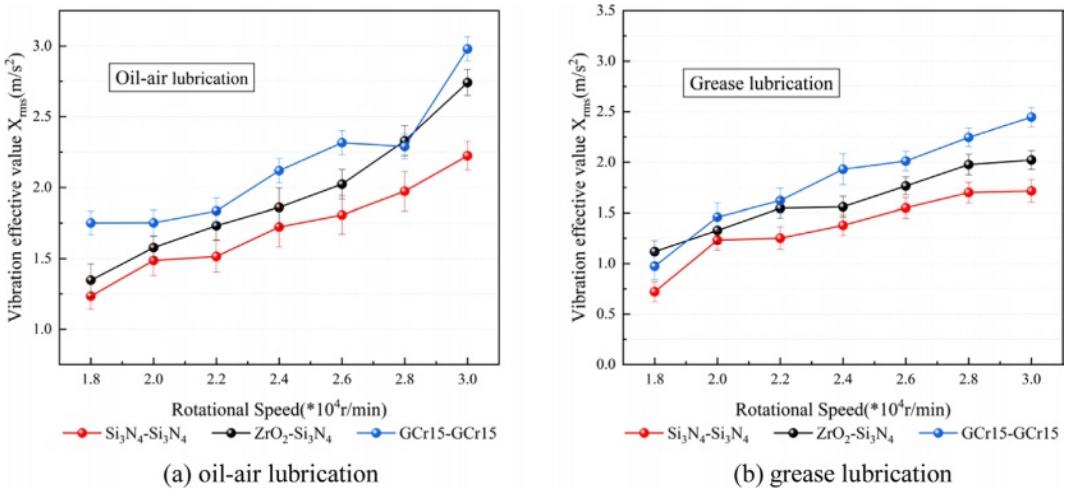

Fig. 8. Influence of rotating speed on bearing vibration under different lubrication methods.

the speed rises to a certain extent, the role of centrifugal force on the silicon nitride ceramic material can be played, greater than the contact force generated by the preload. In addition, due to the large elastic modulus of silicon nitride ceramic material, the stiffness is relatively large, which can effectively inhibit its vibration.

As shown in Fig. 9, the vibration acceleration effective value of grease lubrication is better than that of oil-air lubrication, so the bearing vibration frequency domain under the condition of grease lubrication is analyzed. The relation between motorized spindle speed and rotation frequency can be expressed as:

$$v = \frac{60f}{p} \tag{30}$$

Where: v is the speed, the unit is r/min; f is the frequency, expressed in Hz; p is the number of magnetic poles.

Expressed in the form of frequency, assuming that the rotation frequency of the inner ring of the rolling bearing is f_s, the rotation frequency of the outer ring is f_o, and the relative rotation frequency of the inner ring and the outer ring is f_r, it can be expressed as follows.

$$f_o = 0 \tag{31}$$

$$f_r = f_s = \frac{n}{60} \tag{32}$$

The rotating frequency of the motorized spindle was selected as 300, 350, 400, 450 and 500 Hz corresponding to the rotating speeds 18000, 21000, 24000, 27000 and 30000 r/min for experimental data processing. The amplitude and frequency diagram of the radial vibration acceleration test results of the front bearing of the motorized spindle are shown in Fig. 10. As can be seen from Fig. 10, the rotation frequency of bearings is the main factor in the running process. When the rotation speed is 18000 r/min, first-order frequency (f_r) has a greater impact on the vibration of full ceramic bearing motor spindles, followed by second-order frequency ($2f_r$) and third-order frequency ($3f_r$) for full ceramic bearings of silicon nitride and zirconia. $2f_r$ and $3f_r$ are no different from other vibration signals, relatively stable, and frequency doubling is lower than zirconia ceramic bearings, $2f_r$ has a greater impact on the vibration of steel bearing motorized spindle; in fact, f_r and $3f_r$, this kind of vibration is related to the bearing speed, the number of rolling elements and lubrication methods, at a fixed speed, this kind of vibration is uniform and stable. When the speed is 21000 r/min-30000 r/min, it can be seen that the trend of vibration frequency domain is similar to that of 18000 r/min, and the vibration acceleration at

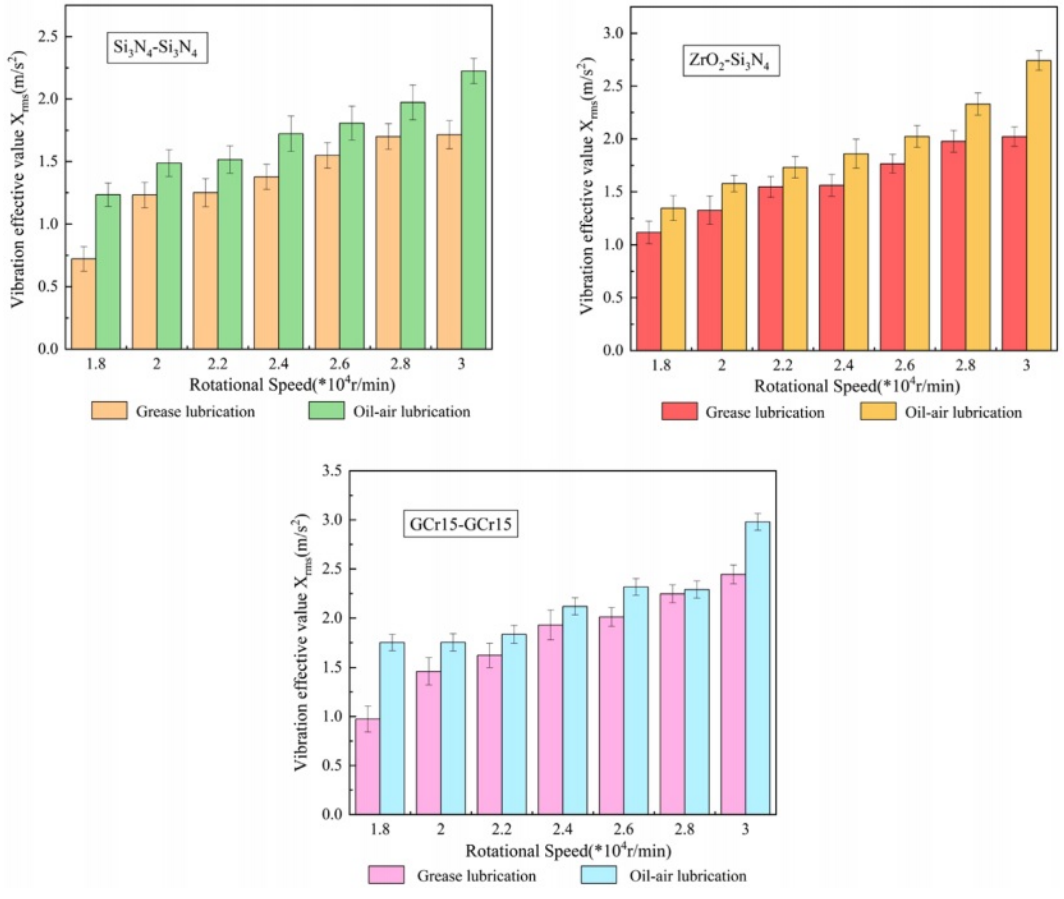

Fig. 9. Comparison of vibration effective values of bearings with different materials under grease lubrication and oil-air lubrication.

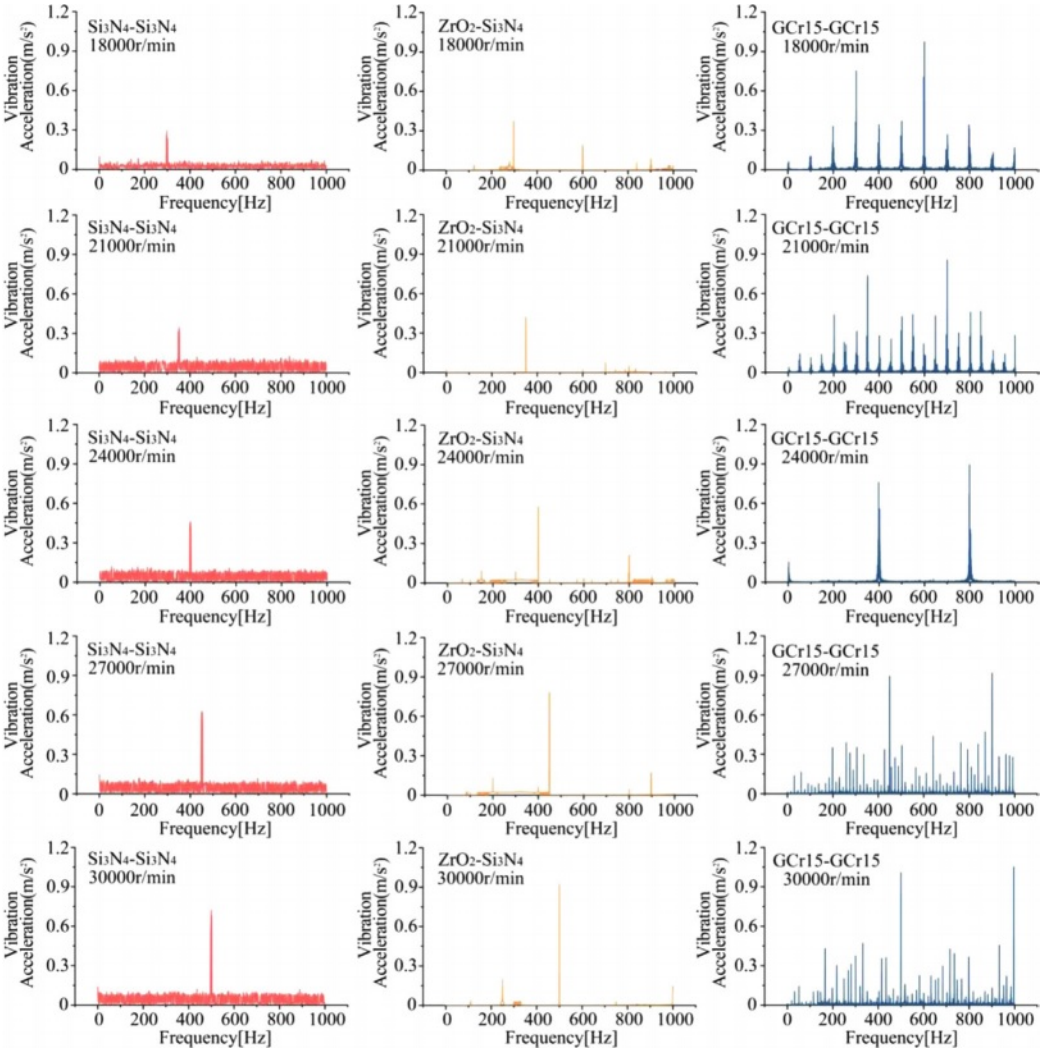

Fig. 10. Vibration frequency domain diagram of high speed bearing motorized spindle system under grease lubrication.

the frequency doubling is increased with the increase of the speed. It can be seen that the vibration frequency domain signal of the full ceramic bearing is relatively stable with the increase of the speed. The vibration frequency domain signal of steel bearing becomes stable when the speed reaches 24000 r/min, and the vibration frequency domain signal floats larger after 24000 r/min. In addition, due to the misalignment of the motorized spindle in the installation error, it will contain a small amount of $2f_r$ and $3f_r$ components. Because $3f_r$ has little influence on the motorized spindle, the influence of f_r and $2f_r$ is shown in Fig. 11.

Analysis of influence of rotating speed on bearing oil film thickness

The relationship between bearing speed and oil film thickness can be calculated in section 3.3. When the bearing is fully lubricated, the influence of different speeds on the oil film thickness in the center of the contact area between the rolling element and the inner ring race is shown in Fig. 12.

As seen in Fig. 12, the thickness of the lubricating oil film formed between the rolling element and the inner and outer race gradually decreases with the increase in bearing speed. When the bearing is running at high speed, a large amount of dense shear heat will be generated at the entrance of the contact zone, resulting in higher oil temperature, lower viscosity, and lower oil film thickness. The contact stress between the rolling body and the inner and outer raceways decreases, and the lubricating oil's film-forming thickness increases with the Angle between the rolling body and the maximum stress point. As shown in Fig. 12, when the position Angle of the rolling element is 180°, the Angle from the maximum stress point is the largest, and the lubricating oil film at this position is the thickest. When the bearing speed is constant, the thickness of the lubricating oil film formed between the rolling body and the inner and outer ring raceways at different position angles is different. Under high-speed conditions, the thickness of the oil film formed by the rolling body in the outer ring is greater than that of the inner ring raceway, because of the action

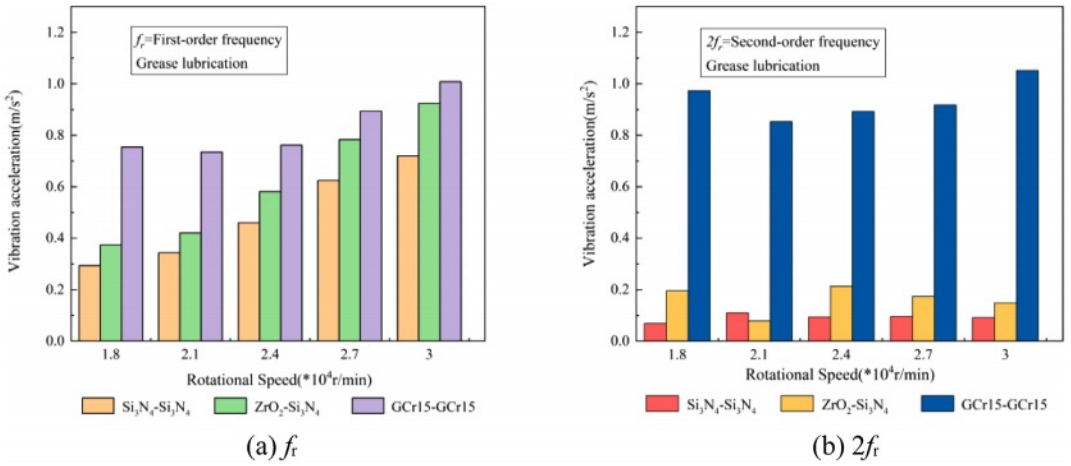

Fig. 11. Influence of frequency doubling on vibration acceleration of ceramic bearing and steel bearing of high speed motorized spindle under grease lubrication.

of centrifugal force, the lubricating oil will move from the center of the bearing to the outer ring, thus forming a thicker oil film. A thinner oil film is formed at the inner ring. By comparing the oil film thickness of the inner and outer raceway contact areas of the three kinds of bearings, it can be found that the oil film thickness of the GCr15-GCr15 bearing is smaller than that of Si_3N_4-Si_3N_4 and ZrO_2-Si_3N_4 bearing when the speed is higher, and the oil film thickness formed by Si_3N_4-Si_3N_4 bearing is the largest. The main reason is that the density of the three materials is different; Si_3N_4 ceramic density is only 41% of GCr15 bearing steel, ZrO_2 ceramic 55%, which leads to the centrifugal force of the ceramic bearing is much less than that of the steel bearing at high speed, the contact force between the rolling body and the raceway is small, and the oil film is thicker.

Analysis of influence of working condition on temperature rise

According to the experimental conditions in Section 2.2, the outer ring of the ceramic bearing in the motorized spindle is equipped with a temperature sensor, and the temperature data of the bearing outer ring is measured and analyzed by the Lion SEA-5 motorized spindle error analyzer. In this experiment, bearing temperature rise was tested at a high operating speed of 18000~30000 r/min. In order to ensure the uniformity of test bearing conditions, the test was carried out from a low speed of 1000 r/min to the measured speed within 15 minutes before reaching the measured temperature and speed, and the test was continued for 1 hour at the measured speed. After testing the cooling time of the motorized spindle at one speed is 1 hour, and then continue to test the next target speed. Due to the large number of test groups, when the rotational speed is 18000, 21000, 24000, 27000 and 30000 r/min respectively, the temperature of the outer ring of full ceramic bearing and steel bearing changes with time under the conditions of oil-air lubrication and grease lubrication respectively, as shown in Figs. 13 and 14.

In the initial stage, full ceramic ball bearings and steel bearings with oil-air lubrication or grease lubrication have a temperature that gradually rises to about a certain temperature to achieve thermal equilibrium. As shown in Figs. 13 and 14, under the conditions of oil-air lubrication or grease lubrication, with the increase of speed, the time for full ceramic ball bearings to reach thermal balance is shorter than that for steel ball bearings to reach thermal balance. As shown in Figure 13, the trend of temperature rise in full ceramic and steel bearings is similar in most initial operating conditions under oil-air lubrication. The higher the rotational speed, the larger the initial temperature peak, and the shorter the time to reach thermal equilibrium. The temperature gap gradually widened, at 27000 r/min and 30000 r/min, the advantages of running 1000s and 750s full ceramic bearings were reflected, and the temperature gap was higher than the previous speed. As shown in Fig. 14, with grease lubrication, the temperature gap between the two kinds of full ceramic bearings becomes smaller as the speed increases, and the full ceramic bearings have obvious advantages over steel bearings at high speed. When the speed below 18000 r/min, with the increase of speed, the thickness of the lubricating oil film formed between the rolling element and the inner and outer ring raceway is gradually increased; However, with the increase of rotational speed, the decrease of viscosity of lubricating oil will lead to the increase of temperature. The decrease of viscosity means that it is more difficult for lubricating oil to form a stable oil film, so the thickness of the oil film will be reduced. Because the oil film thickness of ceramic bearings decreases less than that of steel bearings, the oil film thickness of ceramic bearings at corresponding high speed is larger than that of steel bearings, so the temperature rise is more stable than that of steel bearings, the heat generated is less,

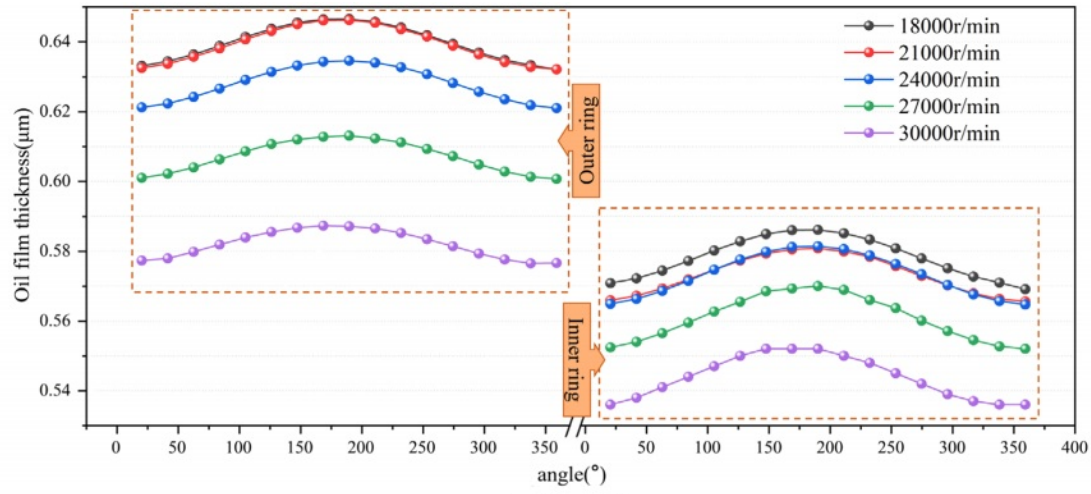

(a) Si_3N_4-Si_3N_4

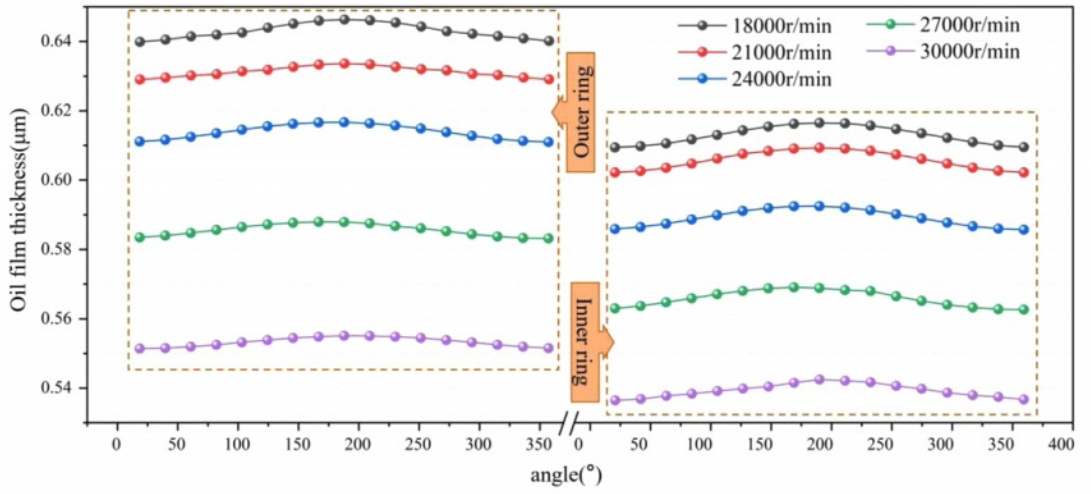

(b) ZrO_2-Si_3N_4

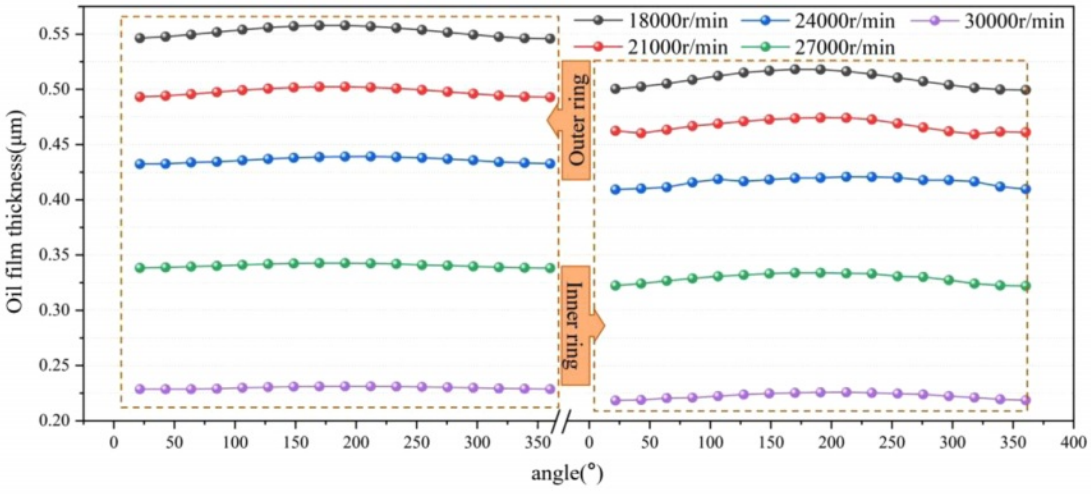

(c) GCr15-GCr15

Fig. 12. The variation of central oil film thickness between different rolling elements and the outer/inner ring racewith rotational speed.

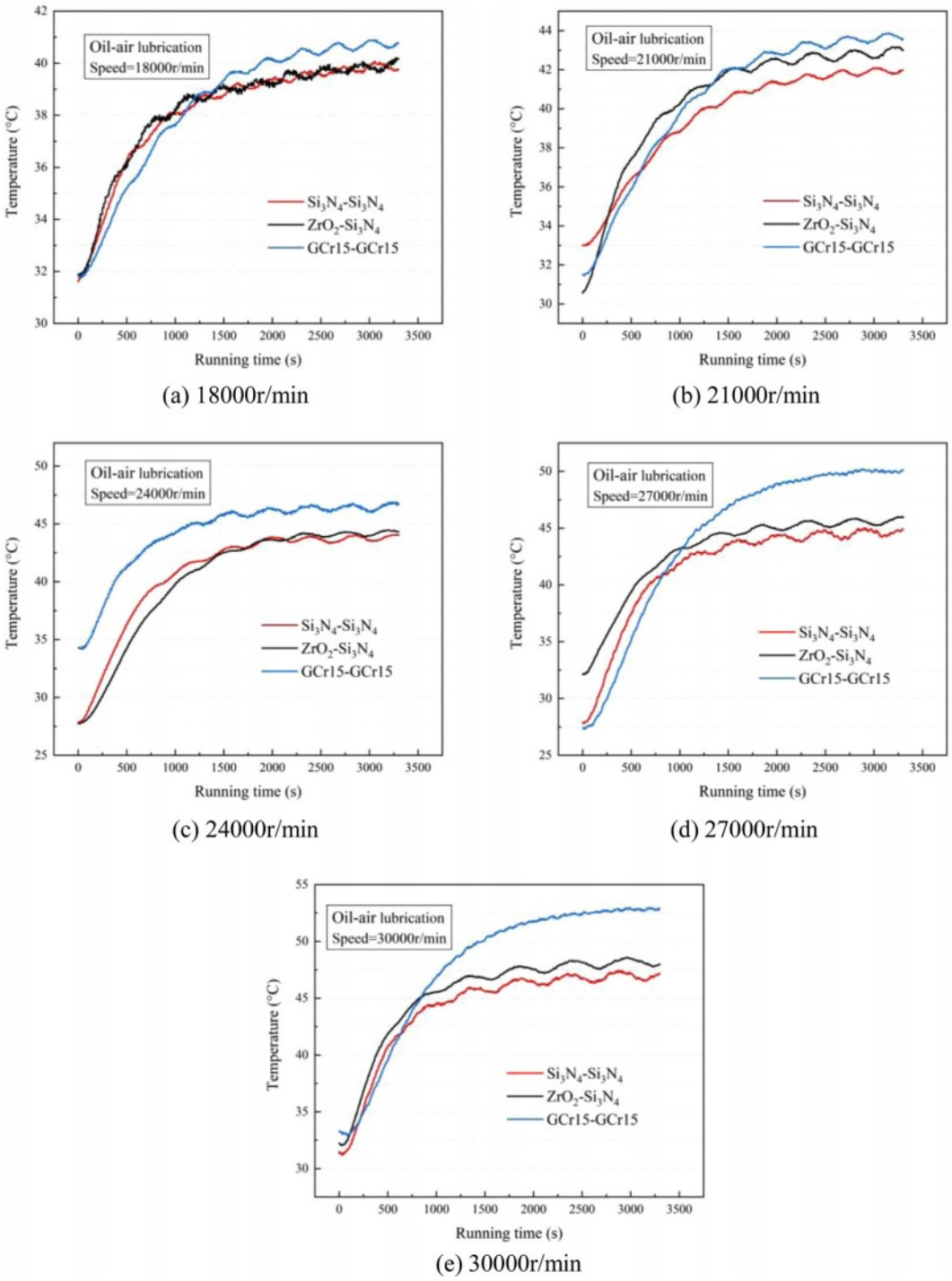

Fig. 13. Bearing operating temperature curve with time under oil-air lubrication.

the difference between heat release and heat output is always small, and the bearing gradually rises to a certain temperature to achieve thermal balance, compared with steel bearings, full ceramic ball bearings can quickly enter the heat balance state.

When the speed over 18000 r/min, if the running time is calculated when the speed rises to the target speed under different lubrication methods before running 1200s, the temperature exhibits a significant rising trend at different speeds. The temperature difference between Si_3N_4-Si_3N_4 and ZrO_2-Si_3N_4 ceramic bearings under oil-air lubrication is small, and the maximum temperature difference is less than 8°C compared with GCr15-GCr15 bearings. In contrast, the temperature difference between Si_3N_4-Si_3N_4 and ZrO_2-Si_3N_4 ceramic bearings under grease lubrication is gradually reduced. However, it is also larger than the temperature gap of oil-air lubrication. Si_3N_4-Si_3N_4 has obvious advantages, and the temperature

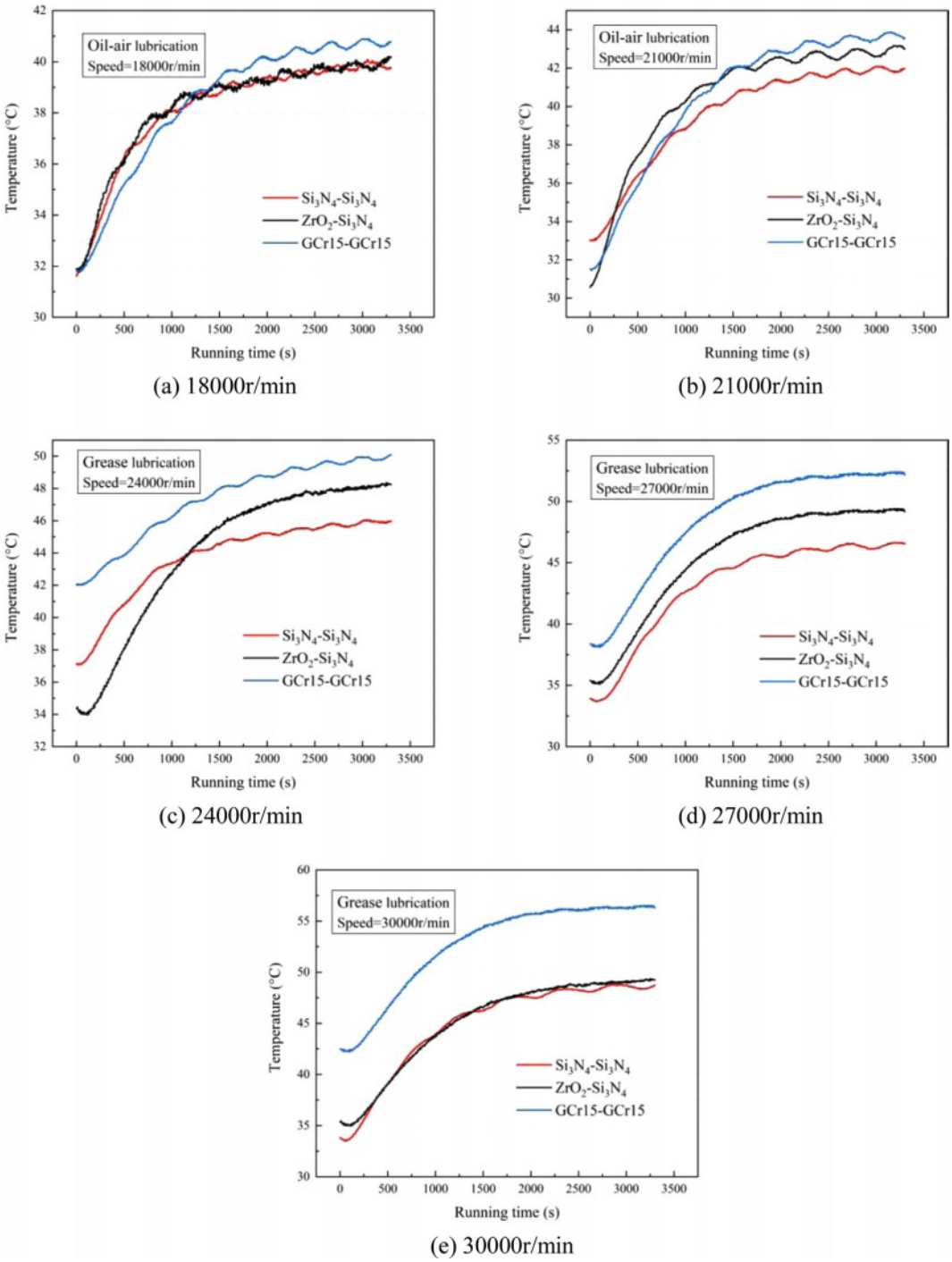

Fig. 14. Bearing operating temperature curve with time under grease lubrication condition.

gap with ZrO_2-Si_3N_4 is within 5°C. The temperature gap with GCr15-GCr15 bearing is within 10°C. Overall, the temperature of oil-air lubrication at high speed is lower than that of grease lubrication. The analysis shows that grease plays a good lubrication role in the bearing. However, the viscosity of grease is relatively large, the shear resistance during bearing operation is high, and the bearing components and environmental media absorb the heat generated by the bearing during grease lubrication. The flowing lubricating oil mainly takes away the heat generated under the condition of oil-air lubrication in addition to absorption and heat transfer by the bearing elements. Hence, the oil-air lubricated bearing is lower than the working temperature of the grease lubricated bearing. At different speeds, the temperature rise of the bearing of the three materials gradually tends to be stable. With the longer running time, the high-temperature resistance and self-lubrication of the full ceramic bearing become more evident so that the performance of the spindle at high speed tends to be stable and the life can

be extended.

Conclusion

In this study, the quasi-static principle and oil film thickness theory were used to analyze the variation trend of centrifugal force and inner and outer raceway center oil film thickness of bearings made of three materials, namely Si_3N_4-Si_3N_4, ZrO_2 -Si_3N_4 and GCr15-GCr15, and controlled variable experiments were conducted on bearings made of the three materials. The vibration and temperature rise of the bearing were studied by changing the speed of the motorized spindle under the condition of controlled lubrication and unchanged bearing material. The following conclusions were drawn:

With the increase of speed, under different lubrication conditions, the vibration RMS of Si_3N_4-Si_3N_4, ZrO_2-Si_3N_4 and GCr15-GCr15 bearing materials generally exhibits an upward trend. Among them, the rising trend of the Si_3N_4-Si_3N_4 full ceramic ball bearing is the most gradual, and its vibration RMS value is the lowest, displaying apparent advantages. The calculated centrifugal force follows the order of Si_3N_4-Si_3N_4 < ZrO_2-Si_3N_4 < GCr15-GCr15 at different speeds, indicating that the centrifugal force is the primary factor causing vibration under high-speed working conditions.

With the increase of speed, the vibration acceleration of full ceramic ball bearing under grease lubrication is lower than that of steel bearing. Meanwhile, f_r exerts a stronger influence on the vibration of motorized spindle of Si_3N_4-Si_3N_4 and ZrO_2-Si_3N_4 full ceramic ball bearing. Among them, the higher the rotating speed of Si_3N_4-Si_3N_4, the lower the other frequency doubling is, and the influence on ZrO_2-Si_3N_4 is $2f_r$ and $3f_r$ in turn, and $2f_r$ has a greater impact on the vibration of steel bearing motorized spindle, followed by f_r and $3f_r$.

At high speed, the temperature rise during oil-air lubrication is lower than that of grease lubrication, with a maximum temperature difference of less than 5°C. As the running time increases, all three types of bearings made of different materials gradually reach thermal balance. Full ceramic ball bearings can achieve thermal balance faster compared to steel bearings. Numerical iterative analysis indicates that the gradual decrease in oil film thickness at the raceway center is the primary cause of temperature rise. Furthermore, the oil film thickness of Si_3N_4-Si_3N_4 bearings is the thickest among the three materials at different speeds, leading to lower temperatures compared to ZrO2-Si_3N_4 and GCr15-GCr15 bearings. These findings provide valuable insights into the lubrication behavior and thermal performance of different bearing materials, and pave the way for future research on optimizing bearing design and lubrication strategies.

Under the same working conditions, the vibration acceleration and temperature rise of full ceramic ball bearing motorized spindle are smaller than that of similar steel bearings. It shows that the dynamic and thermal performance of full ceramic ball bearings is better than that of steel bearings. Among them, Si_3N_4-Si_3N_4 bearing embodies the advantages of dynamic and thermal performance.

Acknowledgments

The authors would like to acknowledge the support of the Key Projects of the National Natural Science Foundation of China (Joint Fund) [grant number U23A20631], Liaoning Province Applied Basic Research Program Project [grant number 2022JH2/101300216] and The Project is sponsored by “Liaoning BaiQianWan Talents Program”, Research Funds of Educational Department of Liaoning Province [grant Number: LJKZ0573].

References

1. T. Li, P. Kolar, X. Li, and J. Wu, Int. J. Precis. Eng. Man. 21 (2020) 163-1185.
2. S. Li, C. Li, M. Liu, Y. Wang, C. Zuo, H. Zhang, and Y Gao, J. Ceram. Process. Res. 24[6] (2023) 1025-1036.
3. L.L. Yang, Z.P. Xie, S. Li, and M. Song, J. Ceram. Process. Res. 35[5] (2014) 457-464.
4. J. Mayr, J. Jedrzejewski, E. Uhlmann, M.A. Donmez, W. Knapp, F. Härtig, K. Wendt, T. Moriwaki, P. Shore, and R. Schmitt, CIRP annals. 61[2] (2012) 771-791.
5. C. Zhang, D. Guo, J. Tian, and Q. Niu, Adv. Mech. Eng. 13[6] (2021) 1-15.
6. H. Liu, Y. Zhang, C. Li, and Z. Li, Nonlinear. Dynam. 105[1] (2021) 131-166.
7. L. Fan, J. Chen, K. Zhang, and L. Zhang, In proceedings of the 29th Chinese Control And Decision Conference (CCDC), IEEE. (2017) 5639-5645.
8. Z. Liu, W. Chen, D. Li, and W. Zhang, Ind. Lubr. Tribol. Int. 69[6] (2017) 1049-1065.
9. Z.J. Y, C. Guo, and X.J. Dong, Journal of Aeronautical Power. 34[10] (2019) 2246-2255.
10. H. Yan, Y. Wu, S. Li, L. Zhang, and K. Zhang, J. Braz. Soc. Mech. Sci. 42[6] (2020) 1-16.
11. J. Sun, Z. Zhang, Z. Xia, X. Fang, R. Guan, G. Zhang, and J. Yao, J. Ceram. Process Res. 24[3] (2023) 541-553.
12. S. Kerst, B. Shyrokau, and E. Holweg, Mech. Syst. Signal. 104 (2018) 384-397.
13. D. Wang, H. Cao, Y. Yang, and M. Du, Mech. Syst. Signal. 191 (2023) 110-152.
14. S. Xi, H. Cao, and X. Chen, Mech. Syst. Signal. 114 (2019) 486-511.
15. I.M. Jamadar and D. Vakharia, Ind. Lubr. Tribol. Int. 70[2] (2018) 264-272.
16. W. Bian, Z. Wang, J. Yuan, and W. Xu, J. Mech. Sci. Technol. 30[1] (2016) 297-306.
17. L. Wang, X. Sheng, and J. Luo, J. Mech. Sci. Technol. 35[2] (2021) 669-678.
18. X. Hao, C. Yu, J. Liu, Q. Han, and Q. Zhai, Journal of Mechanical Engineering. 58[13] (2022) 147-165.
19. Y. Wu, J. Guo, X. Zhang, Y. Zhang, H. Wang, X. Bai, J. Sun, and H. Lu, The International Journal of Advanced Manufacturing Technology. 127[9] (2023) 4943-4957.
20. K. Zhang, Z. Wang, X. Bai, H. Shi, and Q. Wang, Adv. Mech. Eng. 12[1] (2020) 1-18.

21. X.T. Bai, Y.H. Wu, I.C. Rosca, K. Zhang, and H.T. Shi, J. Sound. Vib. 450 (2019) 231-250.
22. H.T. Shi and X.T. Bai, Mech. Syst. Signal. 139 (2020) 106583.
23. D. Zheng and W. Chen, Tribol. Int. 109 (2017) 593-601.
24. L. Wu and Q. Tan, Entropy-Switz. 18[7] (2016) 271.
25. J. Wu, J. Cui, W. Shu, L. Wang, and R. Chen, Tribol. Int. 185 (2023) 108499.
26. Y. Z, X. L, and Q. W, Mechanical Design. 29[3] (2012) 45-49.
27. P. Hou, L. Wang, and Q. Peng, Bulletin of the Polish Academy of Sciences: Technical Sciences [3] (2020) 517-527.
28. J. Liu, R. Pang, Y. Xu, S. Ding, and Q. He, Sci. China. Technol. Sc. 63[6] (2020) 943-952.
29. S. T, and S. B, International Journal of Mechanical Engineering and Technology [8] (2017) 1785-1792.
30. Z. Yang, T. Yu, Y. Zhang, and Z. Sun, Tribol. Int. 105 (2017) 125-134.
31. R. Goraj, Electr. Eng. 99[3] (2017) 861-869.
32. J. Yu, S. Li, X. Chen, L. He, and W. Yuan, Math. Probl. Eng. (2019) 1-15.
33. Z. Xia, Y. Wu, J. Sun, H. Yan, J. Tian, H. Wang, and S. Li, Nonlinear. Dynam. 112[9] (2024) 6947-6966.
34. Y. Zhang, M. Zhang, Y. Wang, and L. Xie, Applied Sciences. 10[8] (2020) 2750.
35. J. Zhang, Y. Zhang, Y. Zhao, and W. Han, Lubricants. 11[5] (2023) 203.